Biomedical Optics EXPRESS

# Assessing breast tumor margin by multispectral photoacoustic tomography

**Rui Li,[1,6] Pu Wang,[1,6] Lu Lan,[1] Frank P. Lloyd Jr.,[2] Craig J. Goergen,[1,5] Shaoxiong Chen,[3] and Ji-Xin Cheng[1,4,5,*]**

[1]*Weldon School of Biomedical Engineering, Purdue University, 206 S Martin Jischke Drive., West Lafayette, Indiana, 47907, USA*

[2] *Surgical Oncology- Cascade Metrix/Putman County Hospital, 1542 S Bloomington Street, Greencastle, Indiana, 46135, USA*

[3]*Department of Pathology and Laboratory Medicine, Indiana University School of Medicine, 350 West 11th Street, Indianapolis, Indiana, 46202, USA*

[4]*Department of Chemistry, Purdue University, 560 Oval Drive, West Lafayette, Indiana, 47907, USA*

[5]*Purdue University Center for Cancer Research, 201 S. University Street, West Lafayette, Indiana, 47906, USA*

[6]*Authors contributed equally*

[*]*jcheng@purdue.edu*

**Abstract:** An unmet need exists in high-speed and highly-sensitive intraoperative assessment of breast cancer margin during conservation surgical procedures. Here, we demonstrate a multispectral photoacoustic tomography system for breast tumor margin assessment using fat and hemoglobin as contrasts. This system provides ~3 mm tissue depth and ~125 μm axial resolution. The results agreed with the histological findings. A high sensitivity in margin assessment was accomplished, which opens a compelling way to intraoperative margin assessment.



**OCIS codes:** (110.5120) General; (000.2700) General science.

## References and links

1. B. Fisher, S. Anderson, J. Bryant, R. G. Margolese, M. Deutsch, E. R. Fisher, J. H. Jeong, and N. Wolmark, "Twenty-year follow-up of a randomized trial comparing total mastectomy, lumpectomy, and lumpectomy plus irradiation for the treatment of invasive breast cancer," N. Engl. J. Med. **347**(16), 1233–1241 (2002).
2. U. Veronesi, N. Cascinelli, L. Mariani, M. Greco, R. Saccozzi, A. Luini, M. Aguilar, and E. Marubini, "Twenty-year follow-up of a randomized study comparing breast-conserving surgery with radical mastectomy for early breast cancer," N. Engl. J. Med. **347**(16), 1227–1232 (2002).
3. R. Arriagada, M. G. Lê, F. Rochard, and G. Contesso, Institut Gustave-Roussy Breast Cancer Group, "Conservative treatment versus mastectomy in early breast cancer: Patterns of failure with 15 years of follow-up data," J. Clin. Oncol. **14**(5), 1558–1564 (1996).
4. J. A. van Dongen, A. C. Voogd, I. S. Fentiman, C. Legrand, R. J. Sylvester, D. Tong, E. van der Schueren, P. A. Helle, K. van Zijl, and H. Bartelink, "Long-term results of a randomized trial comparing breast-conserving therapy with mastectomy: European organization for research and treatment of cancer 10801 trial," J. Natl. Cancer Inst. **92**(14), 1143–1150 (2000).
5. D. Aziz, E. Rawlinson, S. A. Narod, P. Sun, H. L. Lickley, D. R. McCready, and C. M. Holloway, "The role of reexcision for positive margins in optimizing local disease control after breast-conserving surgery for cancer," Breast J. **12**(4), 331–337 (2006).
6. G. A. Cèfaro, D. Genovesi, R. Marchese, L. A. Ursini, E. Cianchetti, E. Ballone, and M. Di Nicola, "Predictors of local recurrence after conservative surgery and whole-breast irradiation," Breast Cancer Res. Treat. **98**(3), 329–335 (2006).
7. M. F. Dillon, E. W. Mc Dermott, A. O'Doherty, C. M. Quinn, A. D. Hill, and N. O'Higgins, "Factors affecting successful breast conservation for ductal carcinoma in situ," Ann. Surg. Oncol. **14**(5), 1618–1628 (2007).
8. N. Cabioglu, K. K. Hunt, A. A. Sahin, H. M. Kuerer, G. V. Babiera, S. E. Singletary, G. J. Whitman, M. I. Ross, F. C. Ames, B. W. Feig, T. A. Buchholz, and F. Meric-Bernstam, "Role for intraoperative margin assessment in patients undergoing breast-conserving surgery," Ann. Surg. Oncol. **14**(4), 1458–1471 (2007).
9. P. I. Tartter, J. Kaplan, I. Bleiweiss, C. Gajdos, A. Kong, S. Ahmed, and D. Zapetti, "Lumpectomy margins, reexcision, and local recurrence of breast cancer," Am. J. Surg. **179**(2), 81–85 (2000).
10. M. C. Smitt, K. Nowels, R. W. Carlson, and S. S. Jeffrey, "Predictors of reexcision findings and recurrence after breast conservation," Int. J. Radiat. Oncol. Biol. Phys. **57**(4), 979–985 (2003).

#233221 - $15.00 USD Received 26 Jan 2015; revised 3 Mar 2015; accepted 5 Mar 2015; published 12 Mar 2015

11. D. E. Wazer, G. Jabro, R. Ruthazer, C. Schmid, H. Safaii, and R. K. Schmidt-Ullrich, “Extent of margin positivity as a predictor for local recurrence after breast conserving irradiation,” Radiat. Oncol. Investig. **7**(2), 111–117 (1999).
12. J. Q. Brown, T. M. Bydlon, L. M. Richards, B. Yu, S. A. Kennedy, J. Geradts, L. G. Wilke, M. K. Junker, J. Gallagher, W. T. Barry, and N. Ramanujam, “Optical assessment of tumor resection margins in the breast,” IEEE J. Sel. Top. Quantum Electron. **16**(3), 530–544 (2010).
13. L. Jacobs, “Positive margins: The challenge continues for breast surgeons,” Ann. Surg. Oncol. **15**(5), 1271–1272 (2008).
14. J. Atkins, F. Al Mushawah, C. M. Appleton, A. E. Cyr, W. E. Gillanders, R. L. Aft, T. J. Eberlein, F. Gao, and J. A. Margenthaler, “Positive margin rates following breast-conserving surgery for stage i-iii breast cancer: Palpable versus nonpalpable tumors,” J. Surg. Res. **177**(1), 109–115 (2012).
15. G. C. Balch, S. K. Mithani, J. F. Simpson, and M. C. Kelley, “Accuracy of intraoperative gross examination of surgical margin status in women undergoing partial mastectomy for breast malignancy,” Am. Surg. **71**(1), 22–27, discussion 27–28 (2005).
16. F. J. Fleming, A. D. K. Hill, E. W. Mc Dermott, A. O’Doherty, N. J. O’Higgins, and C. M. Quinn, “Intraoperative margin assessment and re-excision rate in breast conserving surgery,” Eur. J. Surg. Oncol. **30**(3), 233–237 (2004).
17. T. L. Huston, R. Pigalarga, M. P. Osborne, and E. Tousimis, “The influence of additional surgical margins on the total specimen volume excised and the reoperative rate after breast-conserving surgery,” Am. J. Surg. **192**(4), 509–512 (2006).
18. O. Riedl, F. Fitzal, N. Mader, P. Dubsky, M. Rudas, M. Mittlboeck, M. Gnant, and R. Jakesz, “Intraoperative frozen section analysis for breast-conserving therapy in 1016 patients with breast cancer,” Eur. J. Surg. Oncol. **35**(3), 264–270 (2009).
19. J. C. Cendán, D. Coco, and E. M. Copeland 3rd, “Accuracy of intraoperative frozen-section analysis of breast cancer lumpectomy-bed margins,” J. Am. Coll. Surg. **201**(2), 194–198 (2005).
20. F. D’Halluin, P. Tas, S. Rouquette, C. Bendavid, F. Foucher, H. Meshba, J. Blanchot, O. Coué, and J. Levêque, “Intra-operative touch preparation cytology following lumpectomy for breast cancer: A series of 400 procedures,” Breast **18**(4), 248–253 (2009).
21. A. J. Creager, J. A. Shaw, P. R. Young, and K. R. Geisinger, “Intraoperative evaluation of lumpectomy margins by imprint cytology with histologic correlation: A community hospital experience,” Arch. Pathol. Lab. Med. **126**(7), 846–848 (2002).
22. M. Thill, “MarginProbe: Intraoperative margin assessment during breast conserving surgery by using radiofrequency spectroscopy,” Expert Rev. Med. Devices **10**(3), 301–315 (2013).
23. M. Thill, C. Dittmer, K. Baumann, K. Friedrichs, and J. U. Blohmer, “MarginProbe®--final results of the german post-market study in breast conserving surgery of ductal carcinoma in situ,” Breast **23**(1), 94–96 (2014).
24. H. Pan, N. Wu, H. Ding, Q. Ding, J. Dai, L. Ling, L. Chen, X. Zha, X. Liu, W. Zhou, and S. Wang, “Intraoperative ultrasound guidance is associated with clear lumpectomy margins for breast cancer: A systematic review and meta-analysis,” PLoS ONE **8**(9), e74028 (2013).
25. J. W. Jeong, D. C. Shin, S. H. Do, C. Blanco, N. E. Klipfel, D. R. Holmes, L. J. Hovanessian-Larsen, and V. Z. Marmarelis, “Differentiation of cancerous lesions in excised human breast specimens using multiband attenuation profiles from ultrasonic transmission tomography,” J. Ultrasound Med. **27**(3), 435–451 (2008).
26. T. E. Doyle, R. E. Factor, C. L. Ellefson, K. M. Sorensen, B. J. Ambrose, J. B. Goodrich, V. P. Hart, S. C. Jensen, H. Patel, and L. A. Neumayer, “High-frequency ultrasound for intraoperative margin assessments in breast conservation surgery: A feasibility study,” BMC Cancer **11**(1), 444 (2011).
27. S. Kennedy, J. Geradts, T. Bydlon, J. Q. Brown, J. Gallagher, M. Junker, W. Barry, N. Ramanujam, and L. Wilke, “Optical breast cancer margin assessment: An observational study of the effects of tissue heterogeneity on optical contrast,” Breast Cancer Res. **12**(6), R91 (2010).
28. F. T. Nguyen, A. M. Zysk, E. J. Chaney, J. G. Kotynek, U. J. Oliphant, F. J. Bellafiore, K. M. Rowland, P. A. Johnson, and S. A. Boppart, “Intraoperative evaluation of breast tumor margins with optical coherence tomography,” Cancer Res. **69**(22), 8790–8796 (2009).
29. M. D. Keller, E. Vargis, N. de Matos Granja, R. H. Wilson, M. A. Mycek, M. C. Kelley, and A. Mahadevan-Jansen, “Development of a spatially offset Raman spectroscopy probe for breast tumor surgical margin evaluation,” J. Biomed. Opt. **16**(7), 077006 (2011).
30. M. D. Keller, S. K. Majumder, M. C. Kelley, I. M. Meszoely, F. I. Boulos, G. M. Olivares, and A. Mahadevan-Jansen, “Autofluorescence and diffuse reflectance spectroscopy and spectral imaging for breast surgical margin analysis,” Lasers Surg. Med. **42**(1), 15–23 (2010).
31. A. S. Haka, Z. Volynskaya, J. A. Gardecki, J. Nazemi, J. Lyons, D. Hicks, M. Fitzmaurice, R. R. Dasari, J. P. Crowe, and M. S. Feld, “In vivo margin assessment during partial mastectomy breast surgery using raman spectroscopy,” Cancer Res. **66**(6), 3317–3322 (2006).
32. D. R. Busch, R. Choe, T. Durduran, and A. G. Yodh, “Towards non-invasive characterization of breast cancer and cancer metabolism with diffuse optics,” PET Clin. **8**(3), 345–365 (2013).
33. M. L. Flexman, H. K. Kim, J. E. Gunther, E. A. Lim, M. C. Alvarez, E. Desperito, K. Kalinsky, D. L. Hershman, and A. H. Hielscher, “Optical biomarkers for breast cancer derived from dynamic diffuse optical tomography,” J. Biomed. Opt. **18**(9), 096012 (2013).

#233221 - $15.00 USD Received 26 Jan 2015; revised 3 Mar 2015; accepted 5 Mar 2015; published 12 Mar 2015

34. G. M. van Dam, G. Themelis, L. M. A. Crane, N. J. Harlaar, R. G. Pleijhuis, W. Kelder, A. Sarantopoulos, J. S. de Jong, H. J. G. Arts, A. G. J. van der Zee, J. Bart, P. S. Low, and V. Ntziachristos, "Intraoperative tumor-specific fluorescence imaging in ovarian cancer by folate receptor-α targeting: First in-human results," Nat. Med. **17**(10), 1315–1319 (2011).
35. M. L. Flexman, H. K. Kim, J. E. Gunther, E. A. Lim, M. C. Alvarez, E. Desperito, K. Kalinsky, D. L. Hershman, and A. H. Hielscher, "Optical biomarkers for breast cancer derived from dynamic diffuse optical tomography," J. Biomed. Opt. **18**(9), 096012 (2013).
36. R. Choe, S. D. Konecky, A. Corlu, K. Lee, T. Durduran, D. R. Busch, S. Pathak, B. J. Czerniecki, J. Tchou, D. L. Fraker, A. Demichele, B. Chance, S. R. Arridge, M. Schweiger, J. P. Culver, M. D. Schnall, M. E. Putt, M. A. Rosen, and A. G. Yodh, "Differentiation of benign and malignant breast tumors by in-vivo three-dimensional parallel-plate diffuse optical tomography," J. Biomed. Opt. **14**(2), 024020 (2009).
37. X. Wang, Y. Pang, G. Ku, X. Xie, G. Stoica, and L. V. Wang, "Noninvasive laser-induced photoacoustic tomography for structural and functional in vivo imaging of the brain," Nat. Biotechnol. **21**(7), 803–806 (2003).
38. H. P. Brecht, R. Su, M. Fronheiser, S. A. Ermilov, A. Conjusteau, and A. A. Oraevsky, "Whole-body three-dimensional optoacoustic tomography system for small animals," J. Biomed. Opt. **14**(6), 064007 (2009).
39. J. Laufer, D. Delpy, C. Elwell, and P. Beard, "Quantitative spatially resolved measurement of tissue chromophore concentrations using photoacoustic spectroscopy: Application to the measurement of blood oxygenation and haemoglobin concentration," Phys. Med. Biol. **52**(1), 141–168 (2007).
40. J. W. Kim, E. I. Galanzha, E. V. Shashkov, H. M. Moon, and V. P. Zharov, "Golden carbon nanotubes as multimodal photoacoustic and photothermal high-contrast molecular agents," Nat. Nanotechnol. **4**(10), 688–694 (2009).
41. Q. Zhang, N. Iwakuma, P. Sharma, B. M. Moudgil, C. Wu, J. McNeill, H. Jiang, and S. R. Grobmyer, "Gold nanoparticles as a contrast agent for in vivo tumor imaging with photoacoustic tomography," Nanotechnology **20**(39), 395102 (2009).
42. D. Piras, W. F. Xia, W. Steenbergen, T. G. van Leeuwen, and S. Manohar, "Photoacoustic imaging of the breast using the twente photoacoustic mammoscope: Present status and future perspectives," IEEE J. Sel. Top. Quantum Electron. **16**(4), 730–739 (2010).
43. K. E. Wilson, S. V. Bachawal, L. Tian, and J. K. Willmann, "Multiparametric spectroscopic photoacoustic imaging of breast cancer development in a transgenic mouse model," Theranostics **4**(11), 1062–1071 (2014).
44. S. Manohar, A. Kharine, J. C. van Hespen, W. Steenbergen, and T. G. van Leeuwen, "The twente photoacoustic mammoscope: System overview and performance," Phys. Med. Biol. **50**(11), 2543–2557 (2005).
45. S. A. Ermilov, T. Khamapirad, A. Conjusteau, M. H. Leonard, R. Lacewell, K. Mehta, T. Miller, and A. A. Oraevsky, "Laser optoacoustic imaging system for detection of breast cancer," J. Biomed. Opt. **14**(2), 024007 (2009).
46. J. Folkman, M. Bach, J. W. Rowe, F. Davidoff, P. Lambert, C. Hirsch, A. Goldberg, H. H. Hiatt, J. Glass, and E. Henshaw, "Tumor angiogenesis: therapeutic implications," N. Engl. J. Med. **285**(21), 1182–1186 (1971).
47. B. J. Tromberg, N. Shah, R. Lanning, A. Cerussi, J. Espinoza, T. Pham, L. Svaasand, and J. Butler, "Non-invasive in vivo characterization of breast tumors using photon migration spectroscopy," Neoplasia **2**(1-2), 26–40 (2000).
48. H. W. Wang, N. Chai, P. Wang, S. Hu, W. Dou, D. Umulis, L. V. Wang, M. Sturek, R. Lucht, and J. X. Cheng, "Label-free bond-selective imaging by listening to vibrationally excited molecules," Phys. Rev. Lett. **106**(23), 238106 (2011).
49. R. Li, M. N. Slipchenko, P. Wang, and J. X. Cheng, "Compact high power barium nitrite crystal-based Raman laser at 1197 nm for photoacoustic imaging of fat," J. Biomed. Opt. **18**(4), 040502 (2013).
50. J. R. Rajian, R. Li, P. Wang, and J. X. Cheng, "Vibrational photoacoustic tomography: Chemical imaging beyond the ballistic regime," J. Phys. Chem. Lett. **4**(19), 3211–3215 (2013).
51. B. Wang, A. Karpiouk, D. Yeager, J. Amirian, S. Litovsky, R. Smalling, and S. Emelianov, "Intravascular photoacoustic imaging of lipid in atherosclerotic plaques in the presence of luminal blood," Opt. Lett. **37**(7), 1244–1246 (2012).
52. P. Wang, J. R. Rajian, and J. X. Cheng, "Spectroscopic imaging of deep tissue through photoacoustic detection of molecular vibration," J. Phys. Chem. Lett. **4**(13), 2177–2185 (2013).
53. J. Jaumot, R. Gargallo, A. de Juan, and R. Tauler, "A graphical user-friendly interface for mcr-als: A new tool for multivariate curve resolution in matlab," Chemometr. Intell. Lab **76**(1), 101–110 (2005).
54. L. W. Jerry Workman, *Practical Guide to Interpretive Near-Infrared Spectroscopy* (CRC press, 2007).
55. P. Wang, T. Ma, M. N. Slipchenko, S. Liang, J. Hui, K. K. Shung, S. Roy, M. Sturek, Q. Zhou, Z. Chen, and J.-X. Cheng, "High-speed intravascular photoacoustic imaging of lipid-laden atherosclerotic plaque enabled by a 2-kHz barium nitrite raman laser," Sci. Rep. **4**, 6889 (2014).

## 1. Introduction

Breast-conserving surgery, or lumpectomy, is well accepted for breast cancer treatment [1–4]. To prevent local cancer recurrence after lumpectomy, histology is performed to check whether the excised tumor specimen is surrounded by a sufficient amount of normal tissue [5–8]. If a positive margin, i.e., less than 2 mm between the surfaces of the excised specimen to

#233221 - $15.00 USD Received 26 Jan 2015; revised 3 Mar 2015; accepted 5 Mar 2015; published 12 Mar 2015

the tumor, is identified, then a second operation will be performed to minimize the chance of cancer recurrence [5, 9–13]. Currently, the re-operation rate ranges from 20 to 70 percent [12–17]. Such high re-operation rate highlights a critical need for rapid and highly sensitive intraoperative margin assessment.

**Table 1. Technologies for intraoperative tumor margin assessment. mm: millimeter.**

| Technologies | Sensitivity | Specificity | Depth Resolution | Procedure time | Sensing depth | Ref. |
|---|---|---|---|---|---|---|
| Cytological examination | 80% | 85% | μm | 10 min | Less than 1 mm | [20,21] |
| Frozen section | 73% | 99.6% | μm | 20 min | Less than 1 mm | [18,19] |
| Radio frequency spectroscopy | 71% | 68% | mm | Real-time point detection | A few mm | [22,23] |
| Optical coherence tomography | 100% | 82% | mm | 5 sec per image | ~1 mm | [28] |
| Raman Spectroscopy | 100% | 100% | μm to mm | 1 sec per point | 1-2 mm | [29,31] |
| Diffuse reflectance imaging | 80% | 67% | mm | 30 min for 45 $cm^2$ tissue area | A few mm | [27,30] |
| Ultrasound | 82% | 93% | mm | 20 ms per image | A few centimeter | [24–26] |

From a clinical perspective, examining the excised specimen is the standard of care, whether done intraoperatively or postoperatively. The major criteria for designing an intraoperative margin assessment tool of the excised tissue are [12]: 1) High sensitivity: closely matching the histological result; 2) High speed: obtaining the result in less than 20 min; 3) Deep tissue penetration: imaging up to 2 mm deep in tissue; 4) Large sampling area: detecting the entire margin surface; 5) Removing the need for interpretation from pathologists. Table 1 summarizes the current and emerging technologies for *ex vivo* intraoperative margin assessment, and specifies their speed, sensing depth, resolution, sensitivity and specificity. Cytological examination and frozen section are widely applied clinically, but these two methods suffer from long procedure time and low sensitivity owning to the sampling method [18–21]. Radio frequency spectroscopy reduces the procedure time, but suffers from the sensitivity and specificity due to the lack of chemical selectivity [22, 23]. Intraoperative ultrasound imaging has been applied to guide lumpectomies but with poor chemical selectivity [24–26]. Emerging optical technologies, including diffuse reflectance imaging, optical coherence tomography and spatial offset Raman spectroscopy, have greatly improved the sensitivity and specificity but still suffer from long procedure time, shallow tissue penetration, or an inability to assess the entire tumor tissue [12, 27–31]. Near infrared fluorescence imaging technology has been reported for *in vivo* breast tumor removal [32–34]. This technique requires exogenous labels to specific cancer targets, raising issues of labeling efficiency, toxicity, and regulatory burden. Diffuse optical tomography has also been reported for *in vivo* breast tumor imaging [35, 36]. However, it suffers from poor depth resolution due to a dramatic decrease in depth sensitivity. Therefore, an unmet need exists in developing an intraoperative device that is rapid, sensitive, label-free, and able to scan the entire tissue surface for accurate breast cancer margin assessment.

Photoacoustic tomography (PAT) has proved its capability of rapid deep-tissue imaging with chemical selectivity [37–39]. Current applications of PAT, in the optical window from visible to 950 nm, rely heavily on the contrast from electronic absorption of hemoglobin or exogenous contrast agents [37–41]. With hemoglobin as the contrast, PAT has been used for breast cancer imaging *in vivo* for surgical planning [42, 43]. However, it has not been applied to image excised breast tissue to determine the margin status, partly because the sole contrast

#233221 - $15.00 USD Received 26 Jan 2015; revised 3 Mar 2015; accepted 5 Mar 2015; published 12 Mar 2015

from blood cannot sensitively distinguish tumor from margin tissue [42, 44, 45]. One reason is that hemoglobin is mainly present in angiogenic processes found with invasive cancers but not in ductal carcinoma in situ [46, 47].

More recently, PA imaging has been extended to the second optical window between 1 and 2 microns to explore new contrast such as lipid, which has opened up multiple biomedical applications [46–50]. In this letter, we demonstrate a multispectral PAT system for breast cancer margin detection through multi-spectral excitation between 1100 nm and 1250 nm, where both hemoglobin and fat can be visualized. Our system provides a new means to assess tumor and tumor margin, as hemoglobin indicates angiogenesis while fat is the major form of normal tissue in breast [48–52]. Being able to reach 3 mm imaging depth with 125 μm axial resolution, 100% sensitivity, and speed of 4.5 $cm^2$/min, our method opens a new way to perform intraoperative breast tumor margin assessment.

## 2. Experimental setup

*Multispectral PAT system*

A schematic of our experimental setup is shown in Fig. 1(A). An optical parametric oscillator (OPO) pumped by the second harmonic of a Nd:YAG laser (NT 300, EKSPLA) generates 10 Hz, 5 ns pulses with wavelengths tunable from 670 nm to 2300 nm and with pulse energy ranging from 60 to 100 mJ. The laser output was coupled into a 1.0 cm diameter optical fiber bundle, with two rectangular distal terminals (12 mm × 2 mm) stabilized in parallel on each side of the ultrasound transducer. The pulse energy was ~30 mJ on an illuminated area of 15 mm by 5 mm. The generated ultrasound waves were recorded by a transducer array with 128 elements and 21 MHz center frequency (MS 250, VisualSonics Inc.). The transducer array was placed between the two fiber bundle terminals by a customized holder. Image reconstruction was implemented through a high frequency ultrasound imaging system (Vevo 2100, VisualSonics Inc.). To synchronize pulse excitation and signal acquisition, a function generator (33220A, Agilent) was used to output 10 Hz, 10 μs transistor-transistor logic (TTL) signal and externally triggered the laser and ultrasound system. A delay generator (DG535, Stanford Research System) was deployed for co-registered photoacoustic (PA) and ultrasound (US) dual-modal imaging. An automatic translational stage was applied for scanning the surface of a tumor tissue. The entire image stack covering 16 wavelengths and 12 $cm^2$ tissue area took ~160 seconds. A polyethylene (PE) film phantom was used to characterize the axial resolution of the system (Fig. 1(B)). The result indicated that a full width at half maximum value of ~200 μm was obtained. The axial resolution is proportional to the sound velocity in the medium. Given the sound velocity in polyethylene film and soft tissues is 2.46 km/s and 1.54 km/s, respectively, we expect an axial resolution of 125 μm in soft tissue.

#233221 - $15.00 USD Received 26 Jan 2015; revised 3 Mar 2015; accepted 5 Mar 2015; published 12 Mar 2015

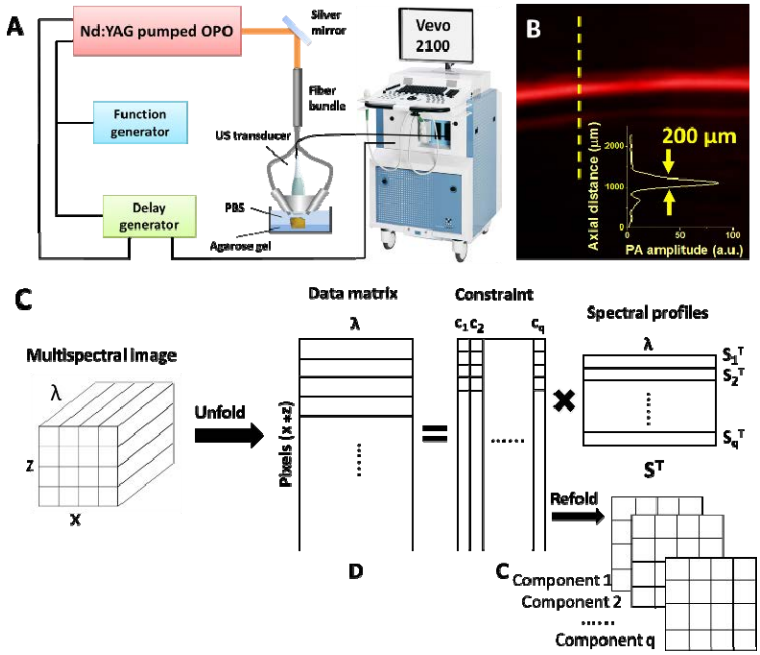


Fig. 1. Multispectral PAT system and multivariate data analysis method. (A) Experimental setup of multispectral PAT. (B) Photoacoustic image of a polyethylene film with 40 µm thickness illuminated at 1210 nm wavelength. (C) Illustration of MCR-ALS analysis.

*Multivariate curve resolution (MCR)*

MCR analysis is performed to extract the compositional information from a multispectral image data set. The MCR model is illustrated in Fig. 1(C). The constructed multispectral image as a 3-D matrix ($x \times z \times \lambda$) was unfolded into a 2-D matrix **D** with the size of (($x \times z$) × $\lambda$), in which the rows were spectra of different pixels. This data set was fit by a bilinear model to produce two matrices, **C** and $\mathbf{S}^{\mathbf{T}}$, plus an error matrix, **E**, expressed as

$$D = CS^T + E \tag{1}$$

Each row in $\mathbf{S}^{\mathbf{T}}$, which had the size ($q \times \lambda$), represented the spectrum of one of the $q$ chemical components. Each column in **C**, which was sized (($x \times z$) × $q$), represented the distribution of one of the $q$ components. The matrix **C** was then refolded to $q$ images, representing distribution maps of $q$ chemical components. An alternating least squares (ALS) fitting algorithm [53] was exploited to solve the MCR bilinear model. This algorithm iteratively optimized the spectral matrix $\mathbf{S}^{\mathbf{T}}$ and the distribution matrix **C**. The data analysis process was performed by a MATLAB package described in reference [53].

*Breast tissue specimens and histology*

The breast tumor samples were excised from a patient diagnosed with invasive ductal carcinoma and then preserved in fixative 10% buffered formalin. The breast tumor was stabilized by 2.5% agarose gel, and placed in a tank filled with phosphate buffered saline solution. After the imaging procedure, the tissue was sectioned and stained with hematoxylin and eosin (H&E) for histological examination.

#233221 - $15.00 USD Received 26 Jan 2015; revised 3 Mar 2015; accepted 5 Mar 2015; published 12 Mar 2015

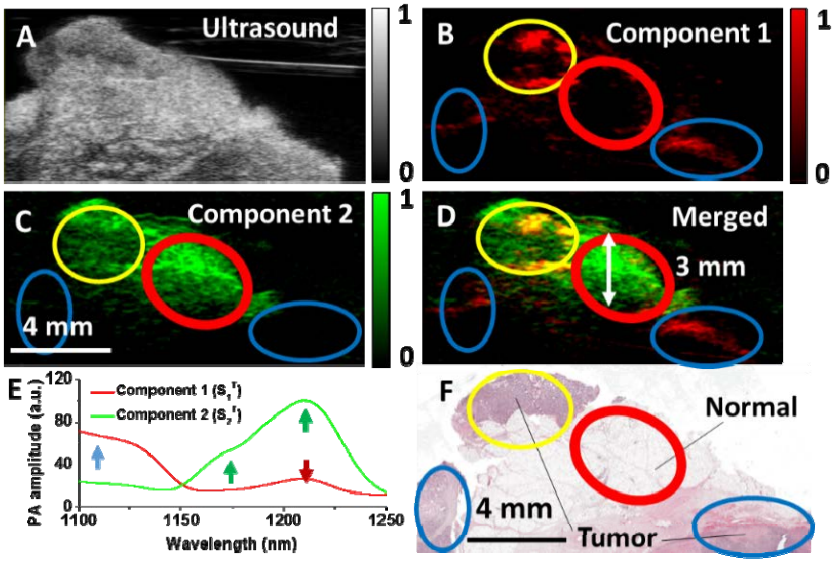


Fig. 2. Spectroscopic PA study of the excised breast tissue from human. (A) Ultrasound image. (B) Image of component 1 showing the hemoglobin contrast. (C) Image of component 2 showing the fat contrast. (D) The merged image indicating an imaging depth of 3 mm. (E) Spectra of components 1 and 2. (F) H&E histology image.

## 3. Results

*Multispectral PAT of excised human breast tissue*

Figure 2 shows the concept of differentiating cancer from normal breast tissue. The B-mode US image shown in Fig. 2(A) identified the tissue morphology. However, the contrast was too vague to distinguish the tumor versus the normal tissue. Multispectral PAT with excitation ranging from 1100 to 1250 nm with 10 nm step size was performed to generate a multispectral image set. By MCR-ALS analysis, two chemical maps were generated from the multispectral image set ($x \times z \times \lambda$), representing two major components in the tissue (Fig. 2(B) and 2(C)). The corresponding spectral profiles of both components are shown in Fig. 2(E). The spectrum of component 1 is mainly contributed by hemoglobin absorption (blue arrow) and second overtone absorption of $CH_2$ group at ~1210 nm (red arrow). The signature peaks of the second overtone of $CH_2$ stretching mode at ~1185 nm and ~1210 nm (green arrow in Fig. 2(E)) in the spectrum of component 2 clearly indicate the presence of fat [54]. Moreover, we found that an imaging depth up to 3 mm was achievable (Fig. 2(D)). Based on the displayed H&E- stained section (Fig. 2(F)) of the same tissue, an area with fat and lacking hemoglobin contrast was assigned to be normal tissue with fat and scattered fibrous tissue (red oval). The area with hemoglobin contrast and fat indicated angiogenesis and invasive tumor with scattered fat tissue (yellow oval). The area without fat contrast indicated tumor tissue with dense fibrous tissue (blue oval). These results collectively demonstrate the capacity of differentiating tumor from fat or fat with fibrous tissue based on the contrast of hemoglobin and fat.

*Breast margin assessment by multispectral PAT*

According to the US image and PA images of the two components generated from the multispectral PAT system, we developed the following protocol to assess the margin status: 1) The ultrasound image was applied to define the boundary of the tissue; 2) The pixel containing fat but no hemoglobin was characterized as normal; 3) The pixel containing both

#233221 - $15.00 USD Received 26 Jan 2015; revised 3 Mar 2015; accepted 5 Mar 2015; published 12 Mar 2015

fat and hemoglobin was considered as tumor; 4) The pixel containing hemoglobin without fat was also considered as tumor. Based on the above criteria, cross-sectional images of normal tissue and tumor tissue were generated. If the tissue area within 2 mm of the surface consisted of 95% normal tissue, we considered it as negative. Otherwise, we classified it as positive. The image analysis was performed with ImageJ.

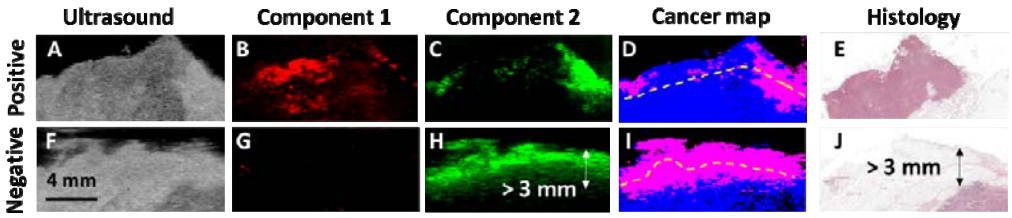


Fig. 3. Distinguishing different types of breast tumor margins. (A, B, C) shows a positive margin imaged by ultrasound and PAT, separately. The analyzed tissue type map with normal tissue in magenta and cancer tissue in blue is shown in (D). The result was confirmed by histological image (E). (F, G, H) shows a typical negative margin imaged by ultrasound and PAT, separately. The analyzed tissue type map is shown in (I). The result was confirmed by histological image (J).

To test the sensitivity and specificity of this method, we performed multispectral PAT on 12 tissues. For these 12 tissues, histological images were independently evaluated by a pathologist. Figure 3 shows the typical positive (Fig. 3(A)-3(E)) and negative (Fig. 3(F)-3(J)) margins. Notably, there was no hemoglobin signal in Fig. 3(F) since the PA imaging cannot reach a depth greater than 3 mm. The tissue maps, which were analyzed based on the above protocol, are shown in Fig. 3(D) and 3(I) with normal and cancer tissue in magenta and blue, respectively. The analysis was only performed in the tissue area within 2 mm from the surface (marked by the yellow dash line). The normal coverage for positive and negative margins is 41% and 98% in Fig. 3(D) and 3(I). The statistical results (Table 2) indicate that 100% sensitivity was achieved. The only false positive case was observed owning to the fact that we did not differentiate dense fibrous tissues from tumor tissue, which led to a reduced specificity.

**Table 2. Results of margin assessment using multispectral PAT**

| | Histology positive | Histology negative |
|---|---|---|
| PAT positive | 7 | 1 |
| PAT negative | 0 | 4 |

## 4. Discussion

*High frequency transducer*

In this study, we used a 21 MHz ultrasound transducer, which was usually less sensitive to lower frequency transducers. However, in breast tumor margin assessment, the current prevailing standard is to check if the tumor is surrounded by 1-2 mm healthy tissue or not. In Fig. 2(D), an imaging depth of up to 3 mm with a signal to noise ratio of 3.5 can be achieved. Therefore, this 21 MHz transducer provides information at sufficient depth while maintaining a better resolution compared to lower frequency transducers.

*The number of wavelengths for tumor margin assessment*

In this study, we applied 16 wavelengths to create a multispectral image set for visualizing hemoglobin and fat. It was critical to apply the spectroscopic imaging study in order to confirm the contrast origin and to demonstrate the feasibility of using hemoglobin and fat for differentiating cancerous and normal tissue. Nonetheless, it is not necessary to record 16 wavelengths for clinical application since hemoglobin and fat have distinctive spectral

#233221 - $15.00 USD Received 26 Jan 2015; revised 3 Mar 2015; accepted 5 Mar 2015; published 12 Mar 2015

profiles. In practice, two wavelengths at 1064 nm and 1200 nm should be enough to distinguish hemoglobin and fat. PAT with 1064 nm excitation has been widely accepted for imaging of hemoglobin in breast tumors because it provides sufficient contrast, enables superior tissue depth penetration compared with visible excitation, and is easily generated through Nd:YAG medium. 1200 nm excitation, where the second overtone of C-H vibration locates, is known for visualization of lipid in deep tissue [48, 52], and is easily generated through an OPO system or a Raman cell [49, 52, 55]. With such dual-wavelength excitation in a mobile system, future clinical application of PAT is promising.

*Sensitivity and specificity*

In lumpectomy procedures, surgeons base the amount of tissue that can be resected on obtaining a good cosmetic result while still achieving negative margins [5]. Therefore, maximizing the sensitivity in breast tumor margin assessment is essential. In this study, we applied a classification rule that only fatty tissue with scattered connective tissue is considered as normal tissue. As a result, 100% sensitivity was achieved. In our study, as a trade-off to the high sensitivity, the dense connective tissue was also characterized as cancer in one case, which led to a reduced specificity of 75%. However, given the mechanical property differences between the dense connective tissue and cancer tissue, frequency analysis of their photoacoustic signals can be applied to improve the specificity.

*Imaging speed*

Our system can assess the surface of the entire tumor tissue with a speed of 4.5 $cm^2$/min when 16 wavelengths are applied. This results in a 3-D multispectral image ($(x \times y \times z) \times \lambda$). As discussed, if 2 or 3 wavelengths are applied, the speed can be further improved. Theoretically, with a 10 Hz laser, 15 mm x 5 mm illumination area, 200 μm translational step size, and 2 wavelength excitation, the speed can reach ~36 $cm^2$/min, making multispectral PAT a rapid tool for assessing the entire excised tissue surface.

## 5. Conclusion

We have demonstrated a multispectral PAT system, which assesses the margin status of excised human breast tissue. This system has sub-millimeter axial resolution, mm-scale deep tissue penetration and high imaging speed. For margin assessment during lumpectomy procedures, further developments of the PAT system are needed to improve the imaging speed, laser compactness, and specificity of the assessment.

## Acknowledgments

This work was partly supported by National Innovation Award from American Heart Association and Walther Cancer Foundation to JXC from the Purdue Center for Cancer Research. This work was partly supported by the American Heart Association (14SDG18220010 to CJG). Also, we would like to thank VisualSonics Inc. for support in the development of photoacoustic tomography in the second optical window.